IRANIAN JOURNAL OF CATALYSIS

# The most important parameters that affect the photocatalytic activity of ZnO nanostructures against organic dyes: A Review

**Marwa Jawad Kadhim[a,*], Mazin Auny Mahdi[a,*], Abbas Mohammed Selman[b], Salwan Kamal Jamel Al-Ani[c], Jalal Jabar Hassan[a], Naser Mohammed Ahmed[d]**

*a) Department of Physics, College of Science, University of Basrah, Basrah, Iraq*
*b) Department of Pharmacognosy and Medicinal plants, Faculty of Pharmacy, University of Kufa, Najaf, Iraq.*
*c) Department of Physics, College of Science, Al-Mustansiriya University, Baghdad, Iraq*
*d) School of Physics, Universiti Sains Malaysia, Gelugor, Penang, Malaysia*

Received 15 October 2022; received in revised form 30 December 2022; accepted 31 January 2023 (**DOI: 10.30495/ijc.2023.1969439.1966**)

ABSTRACT

Organic dyes are among the main sources of water pollution that cause serious health problems for living organisms. Removing dye pollution from water sources is important because of its high toxicity, so it has attracted the interest of researchers. Heterogeneous photocatalysis based on ZnO is one of the most important methods of pollution treatment. The purpose of this review is to summarize the use of ZnO nanostructure and ZnO modified as photocatalysts. The studied mechanism of dye photocatalytic activity and the most important factors affecting the photocatalytic process are discussed. The major effective parameters associated with the surface and morphology to look upon for the efficient photodegradation of organic pollution are structural and average particle size, surface area, band gap crystalline structure, surface density, and porosity. The photodegradation reactions depend on the state of ionization as well as on the surface charge of the photocatalyst and organic dye because pH will determine the charge of the catalyst according to the medium. On the other hand, the calcination temperature was increased throughout the work to break down the pores, which reduces the surface area of the synthesis photocatalyst. The type of dye has an important influence on the success of the photocatalytic process.

***Keywords**: ZnO, Photocatalytic activity, Organic dyes, Photodegradation*

**List of content**



*Corresponding author:
E-mail address: marooj2013@gmail.com (**M. J. Kadhim**); m.a.mahdi@uobasrah.edu.iq (**M. A. Mahdi**)

## 1. Introduction

### *1.1 Organic pollutants*

Direct disposal of industrial compounds into the water makes it unsuitable for drinking and other purposes. In particular, non-biodegradable and undesirable chemicals have negative consequences on the health of humans and aquatic life. Polluted water causes diseases in humans, leading to the deaths of a few million people every year, and the death ratio will be increase in the coming years because of the increased pollution of water [1]. Organic pollutants are the most prevalent and have a negative impact on the environment due to their multiple sources. However, dyes are a class of organic pollutants causing notable environmental pollution released by many industries, with an estimation of more than $7 \times 10^5$ tons of dyes produced per year, and around 10% of this is released to the environment [2]. These dyes prevent the reoxygenation capacity of water

bodies, which results in the stoppage of most biological activity in aquatic life. Conventional water treatment methods, such as coagulation, flocculation, sedimentation, filtration, and disinfection, which are used for water purification are dangerous for public health and are not capable of removing these hazardous materials from water [3, 4].

*1.2 Photocatalysis process*

The Photocatalysis process has received high attention for wastewater treatment due to its green method used sunlight to disintegrate chemical contaminants and organic dyes. There are two main advantages of photocatalysis. First, the reaction conditions such as sunlight, room temperature, and normal atmospheric pressure are readily available, and second, the degradation process is pollution-free, producing no harmful products or by-products [5]. Metal and metal oxide nanoparticles exhibit good photocatalytic properties for the degradation of such chemicals, where the photocatalyst works through oxidation and reduction processes via trapping light energy, which leads to the quick degradation of the pollutants [6]. Metal oxides such as $TiO_2$ [7], $Fe_3O_4$ [8], $Cu_2O$ [9], and $WO_3$ [10] are widely used as photocatalysts. These photocatalysts are environmentally friendly materials, effective, with a low cost [11], and capable of photodegradation of harmful and toxic chemical compounds [12]. However, although it is the wide use using of $TiO_2$ nanostructures for many applications but still appears some limitations due to poor adsorption where a limited amount of sunlight (2–3%) is absorbed and there is a tiny surface area. Furthermore, the $TiO_2$ nanoparticle's ability to aggregate is a problem for some applications in addition to the collection of it from the suspension following the catalytic reactions is a further problem to be resolved for the catalyst application of $TiO_2$ nanoparticles [13], [14]. Furthermore, heterogeneous photocatalysis could lead to enhancing the photodegradation ratio, reducing time as well as using visible light. S. Vahabirad and A. Nezamzadeh-Ejhieh found high efficiency of the photocatalysis in SSZ removal by $BiOI/(BiO)_2CO_3$ binary under visible light compared by BiOI, and $(BiO)_2CO_3$ photocatalysts [15]. CdS/CuO nanoparticles is also used to remove MB dye under visible light and the photodegradation ratio could be reached 83% after 80 min of irradiation [16].

*1.3 Zinc Oxide (ZnO) nanostructures*

Since 2000, researchers' interest in the metal oxide zinc oxide (ZnO) has increased because the preparation of this compound is easy in many types of nanostructures [17], using different methods such as solvothermal [18], hydrothermal [19], chemical bath deposition [20], sol-gel [21], and mechanical technique [22]. ZnO is a semiconductor that belongs to group II-VI and has an excitation energy of 60 meV with a wide bandgap of 3.37eV [23]. However, Ghattavi and Nezamzadeh-Ejhieh reported a bandgap of ZnO prepared is 3.27 eV by hydrothermal method [24]. ZnO has chemical stability, a friendless environment, easy synthesis in nanostructured forms, and low-cost material [13, 19]. Furthermore, ZnO is easy to grow as a nanorod, which has a very high surface-to-volume ratio [25] and weakly visible light absorption compared to the UV region [25]. ZnO nanoparticles (NPs) have a distinct market niche due to a number of appealing characteristics, including the ability to remove organic contaminants at a low cost of manufacturing [26]. However, ZnO nanorods also have high surface defects and thus have shown high photocatalytic performance [27]. ZnO nanostructures have unique electrical and optical properties, which led to their use in a lot of different things, like UV detectors [28], gas sensors [25], [29] biosensors [30] supercapacitors [31], photovoltaic [32], and solar cell [33], etc. However, using ZnO nanostructures as a photocatalysis to degrade many types of organic dyes represented an important application of this material, especially its appearance and excellent photocatalytic activity for environmental treatment and organic pollutants [29, 30]. As stated above, ZnO is more effective for the photodegradation of different organic dyes such as Methylene Blue (MB) [36], Methylene Orange (MO), Rudman B (RB) [37], crystal violet [38], and malachite green [39]. Consequently, the photocatalytic activity of ZnO can be affected by different parameters such as surface morphology [40], and surface oxygen vacancy concentration [41]. However, photocatalytic efficiency was decreased significantly with the recombination of (electron-hole) photogenerated pairs and this is considered as a major problem problem major of this process [42].

The present review article discusses the important parameters that affect the photocatalytic activity of ZnO nanostructures, such as morphology, the calcination temperature, pH of the solution, type of dye, catalyst loading, as well as light intensity, and wavelength.

## 2. Photocatalytic Degradation Mechanism of Dyes by ZnO

The mechanism of photocatalysis started when the photocatalyst material absorbs photons from any light source. When an incident photon has energy (hυ) equal to or higher than the band gap ($E_g$) of an irradiated photocatalyst, electrons excite from the valance band (VB) to the conduction band (CB) leaving holes to form ($e^-$-$h^+$) pairs. The high oxidation potential of electrons in

CB allows direct oxidation of dye in the reaction medium followed by the degradation process. Dye decay is caused by its interaction with free radicals (hydroxyl ($OH^{\cdot}$) and superoxide ($O_2^{\cdot -}$) that produced by the catalyst as seen in **Fig.1**. For the ZnO photocatalyst, interaction is shown in the following equations [7, 8]:

$$ZnO + h\upsilon \rightarrow ZnO\ (e_{CB}^{-} + h_{VB}^{+}) \quad 1$$

$$ZnO(h^{+}) + H_2O \rightarrow ZnO + H^{+} + OH^{\cdot} \quad 2$$

$$ZnO(h^{+}) + OH^{-} \rightarrow ZnO + OH^{\cdot} \quad 3$$

$$ZnO(e^{-}) + O_2 \rightarrow ZnO + O_2^{\cdot -} \quad 4$$

$$O_2^{\cdot -} \xrightarrow{H^{+}} HO_2^{\cdot} \ \ldots \quad 5$$

$$pollution + h^{+} \rightarrow oxidation\ products \quad 6$$

$$pollution + e^{-} \rightarrow reducation\ products \quad 7$$

$$pollution + OH^{\cdot} \rightarrow degradation\ prodact \quad 8$$

However, photocatalyst reactions are allowed by the band energy position of ZnO and the redox potentials of the adsorbates. In the reduction mechanism, the redox potential of the adsorbate is below the conduction band of the ZnO leading to the transfer of excited electrons from the conduction band to the adsorbed particle. In the oxidation mechanism, the redox potential of the adsorbate is above the valence band of ZnO to donate an electron to the vacant hole in the valence band. The equation above concluded of the powerful reducing agents that can start the pollutants degradation through the reduction process are photoinduced electrons. On the other hand, the photoinduced holes are the strong oxidizing agents that can quickly attack organic contaminants and oxidize them to start the process of degradation. The dissolved oxygen can be indirectly reduced by the photoinduced electrons to produce the potently reactive superoxide radicals. While, the photoinduced holes might attack water molecules or hydroxyl anions to produce hydroxyl radicals, which act as potent agents of oxidization. These radicals attack powerful molecules organic and photodegrade them into carbon dioxide, water, and other inorganic species or harmless intermediates [43–47]

The ZnO photocatalyst is activated by UV light due to its wide band gap of 3.37 eV, λ = 368 nm) [48]. The visible-light-activated ZnO has attracted much attention because the solar light spectrum includes only 5% UV light, as well as artificial room lighting, also emits visible light. Therefore, to get of high photocatalysis rate and overcome all challenges under visible light irradiation, the ZnO nanostructure has been modified by doping alkaline earth metals such as Mg [49], or transition metal NP doping such as Fe [50]. Furthermore, noble metal NPs such as Ag, and Au [40–42], as well as non-metals like sulfur (S) and carbon (C) [54], [55] are used to modify ZnO to work as a photocatalyst under visible light irradiation. The modification of the semiconductor surface with metal nanoparticles enhances photocatalysis through two phenomena that can occur at the interface of metal/semiconductor which is surface plasmonic resonance (SPR) and Schottky barrier formation [56]. For example, in coupling Ag metal with ZnO, the CB of Ag is overlapped with VB thus, electrons will move from Ag to ZnO until the Fermi levels of Ag and ZnO is at the same level. Moreover, the modification of ZnO nanostructure can be happened using other semiconductors has an energy band gap less than ZnO such as $V_2O_5$ as shown in **Fig. 2** a and b.

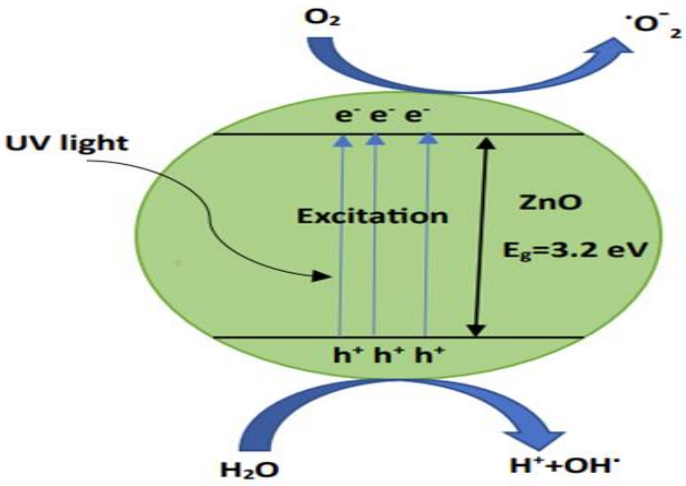


**Fig 1.** Mechanism of the photocatalytic process of degradation by ZnO under Uv-irradiation.

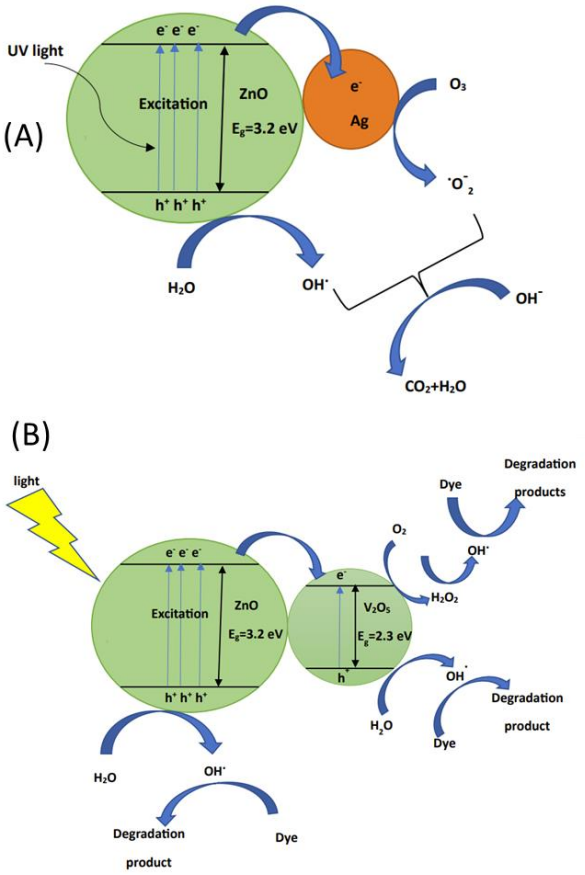


**Fig 2.** Visible light induced charge separation mechanism of photovatalytic of (a) Ag/ZnO (b) ZnO/$V_2O_5$.

The photoelectrons on the Ag surface and CB of ZnO can be trapped by $O_2$ molecules in water and transferred to $O_2^-$ while the photo holes on VB for the semiconductor react with $OH^-$ to produce radical hydroxyl [57]. Further, the recombination process will be restricted by transferring electrons to organic materials in solution by defects at the Ag/ZnO interface, as seen in **Fig. 3**, which illustrates the photodegradation mechanism of Ag/ZnO photocatalysts under irradiation by sunlight against metronidazole (MNZ) pollution. So, photoelectrons will absorb by $Ag^+$ and be reduced to Ag as well as all active oxygen species, and $h^+$ can degrade pollution. The interaction can be described by [57]:

$$e^- + Ag^+ \rightarrow Ag \quad (9)$$

$$O_2^{\cdot -}/OH^{\cdot}/h_{VB}^+ + pollution \rightarrow degradation\ prodact \quad (10)$$

Photocatalysis can mineralize organic dyes fully to $CO_2$, $H_2O$, and mineral acids without bringing secondary pollution [11]. Moreover, photons having an energy greater than the ZnO energy gap will create photoexcited electron-hole pairs, and the electrons in the VB will depart and transfer to CB, leaving the VB with the same number of h+. This system allows electron shift from the conduction band to the valence band to minimize the risk of the exciton recombination process and the target for the reduction of organic pollutants [58]. In this state, the photocatalysis process depends on the creation of charge carriers in both the valence band (VB) and conduction band (CB) which the potentials of the CB and the VB edges of both binary semiconductors photocatalyst can be calculated by using Mulliken electronegativity theory as formula follows [59]:

$$E_{CB} = X - E_e - 0.5E_g \quad (11)$$

$$E_{VB} = E_{CB} - E_g \quad (12)$$

Where $E_{CB}$ and $E_{VB}$ are the positions of CB and VB potential of the photocatalyst, respectively. The X is the electronegativity of the semiconducting photocatalyst which was 5.79 eV for ZnO. $E_g$ is the energy band gap of the semiconducting photocatalysts. $E_e$ is the free electron energy on the standard hydrogen potential (≈4.5) eV. Each atom's electronegativity was calculated by half the total of each element's first ionization energy and electron affinity [60]. The Mulliken electronegativity approach has been widely used to calculate the band edges of semiconductors and quickly grasp the properties of the structure band for a given Eg and composition of the sample [61].

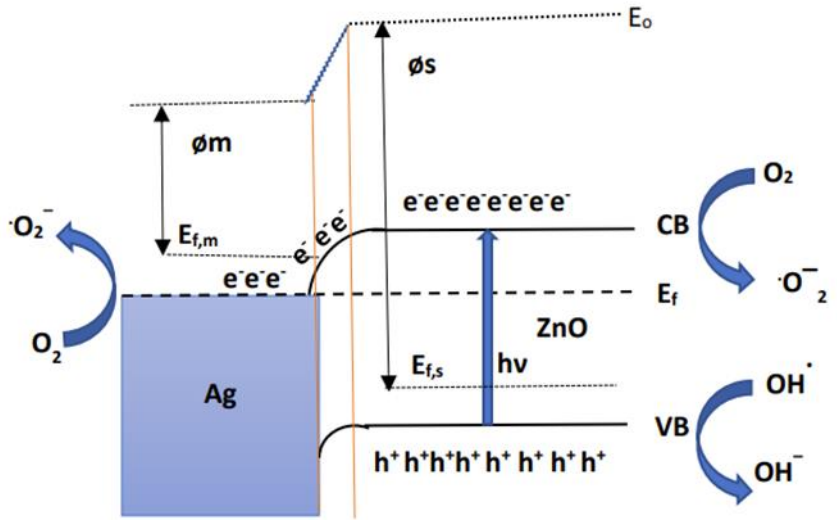


**Fig 3**. Proposed band structure and photocatalytic mechanism of Ag/ZnO

Many types of semiconductors have been used to fabricate heterojunction with ZnO, such as cadmium sulfide (CdS) which has an optical band gap of 2.52 eV (~492 nm) [62]. The charge carrier pairs are photogenerated after light irradiation of the ZnO/CdS photocatalyst. The photoelectrons would be moved from the CB of CdS to the CB of ZnO because the edge potentials of CB and VB for CdS are more negative than the CB and VB of ZnO. The CB and the VB potentials of CdS are − 0.65 eV and 1.75 eV respectively, while those of ZnO are − 0.33 eV and 2.91 eV, respectively [63]. Photogenerated electrons could then react with adsorbed oxygen on the surface of the photocatalyst to form ( $O_2^{\cdot -}$) radicals that could then produce the ($OH^{\cdot}$) radical in the system. On the other hand, the photogenerated holes in the VB of CdS could also oxidize the organic dyes directly due to the intrinsic oxidation capacity of the photo holes [63]. The reaction mechanism can be proposed as shown below [51, 52]

$$ZnO/CdS + h\nu \rightarrow ZnO/CdS\ (e_{CB}^{-} + h_{VB}^{+}) \quad 13$$

$$ZnO(e_{CB}^{-}) + O_2 \rightarrow O_2^{\cdot -} \quad 14$$

$$O_2^{\cdot -} + H_2O \rightarrow\ OH_2^{\cdot} + OH^{-} \quad 15$$

$$OH_2^{\cdot} + H_2O \rightarrow\ H_2O_2 + OH^{\cdot} \quad 16$$

$$H_2O_2 \rightarrow 2OH^{\cdot} \quad 17$$

$$OH^{\cdot} + dye \rightarrow CO_2 + H_2O \quad 18$$

Otherwise, the photoelectrons would be moved from the CB of ZnO to the CB of the $V_2O_5$ photocatalyst according to the Mulliken electronegativity theory, because the CB and the VB potentials of the $V_2O_5$ were 0.46 and 2.47 eV, respectively, as those of the ZnO were 0.35 and 2.93 eV, respectively [66]. The whole mechanism of photocatalysis by oxidation/reduction can be described as [66]:

$$ZnO/V_2O_5 + h\nu \rightarrow\ ZnO/V_2O_5(e_{CB}^{-} + h_{VB}^{+}) \quad 19$$

$$ZnO(e_{CB}^{-}) \rightarrow V_2O_5(e_{CB}^{-}) \quad 20$$

$$ZnO(h_{VB}^{+}) \rightarrow V_2O_5(h_{VB}^{+}) \quad 21$$

$$V_2O_5(e_{CB}^{-}) + H^{+} + O_2 \rightarrow H_2O_2 \quad 22$$

$$H_2O_2 +\ e^{-} + h\nu \rightarrow OH^{\cdot} + OH^{-} \quad 23$$

$$OH^{\cdot} + h^{+} + dye \rightarrow Degradation\ proudacts \quad 24$$

Composite photocatalysts with a p-n junction structure have been intensively explored in recent years. According to the studies, the photoexcited charge carrier pairs are efficiently separated due to the action of the internal electric field in the p-n junction, leading to a huge increase in photocatalytic activity. The experimental results revealed that when the amount of p-type semiconductor crosses a particular threshold, the photocatalyst's activity is drastically reduced [67]. Sun et al. fabricated p-$TiO_2$/n-ZnO photocatalysts and they found that the photocatalytic activity increased with the amount of $TiO_2$ when ZnO is the primary part of the heterojunction photocatalysts. However, the photocatalytic activity decreases rapidly with the increase of ZnO when $TiO_2$ is the main part of the n-ZnO/p-$TiO_2$ heterojunction. This behavior could be induced by various photogenerated electron and hole migration processes and separation mechanisms for ZnO/$TiO_2$ heterojunction with different major components [67]. Moreover, the inner electric field in the interface acted as a potential barrier to retard the recombination of photogenerated charge carrier pairs. Dong et al. [68] prepared $Co_3O_4$/ZnO core/shell heterojunction and found enhancement enhancing in the

photocatalytic performance because of the efficient separation of photogenerated charge carrier pairs at the p-n junction compared by a single component photocatalysts [68]. The inner electric field affected by the holes flows into the negative field while the electrons move to the positive field and the photo charge carrier pairs will be separated effectively by the p–n junction [69]. For example, when the structure is n-$TiO_2$/p-ZnO, in this case, the photoelectrons of the p-ZnO CB will be moved to the CB of $TiO_2$ while the photoelectrons of $TiO_2$ will remain in the CB of $TiO_2$ and the holes will move in the opposite direction from the electrons. However, the enhancement of photocatalytic performance of the p-ZnO/n-$TiO_2$ is attributed to inner electric field-assisted charge transfer at the junction interfaces between the semiconductors with matching band potentials, which then favors an active photoexcited charge carrier separation in the two semiconductors [69]. **Fig. 4a** represented of high Photocatalytic activity of ZnO/$Fe_3O_4$ thin films comparison with ZnO against MB dye under visible light irradiation and noted degradation rate of ZnO/$Fe_3O_4$ is 100% at 180 min while ZnO is 28% at 240 min. **Fig. 4b** shows the activity of ZnO and ZnO/FeO as photocatalysts of degradation wastewater, the latter compound was more effective under visible light than ZnO without modification at 140 min. An interesting composite structure of AgI/$WO_3$/ZnO was prepared and investigated as a photocatalyst to remove MB dye under visible irradiation. The photodegradation ratio reached to 79% after 40 min of irradiation when the composite ratio was 2:1:1 of the compounds AgI/$WO_3$/ZnO[70]. **Table 1** shows various types of dopants and coupling that were previously employed to synthesize ZnO nanostructures as well as their photocatalytic applications.

## 3. Parameters Affecting the Photocatalytic Efficiency

### *3.1 Surface Morphology*

The modifying surface shape of the metal oxide photocatalyst can lead to more efficient dye degradation [71]. Surface influence can be a significant operator for heterogeneous photocatalysis due to the coordination and order of surface atoms that fundamentally determine the adsorption of the reactant onto the surface of the molecules, and also the distribution of the surface between the photoexcited electron and the reactant molecules, and product molecules [72]. The optimum photocatalyst concentration should be specific for heterogeneous photocatalysis systems to avoid the scattering light and concentration effect of the uncovered photocatalyst surface. Thus, without achieving an optimum photocatalyst, the absorption of photons will be weak, leading to a decrease in the rate of decay [73]. The surface morphology of the catalyst, especially those that have a large surface area, can be an influential and decisive factor in getting the highest photocatalytic efficiency [74].

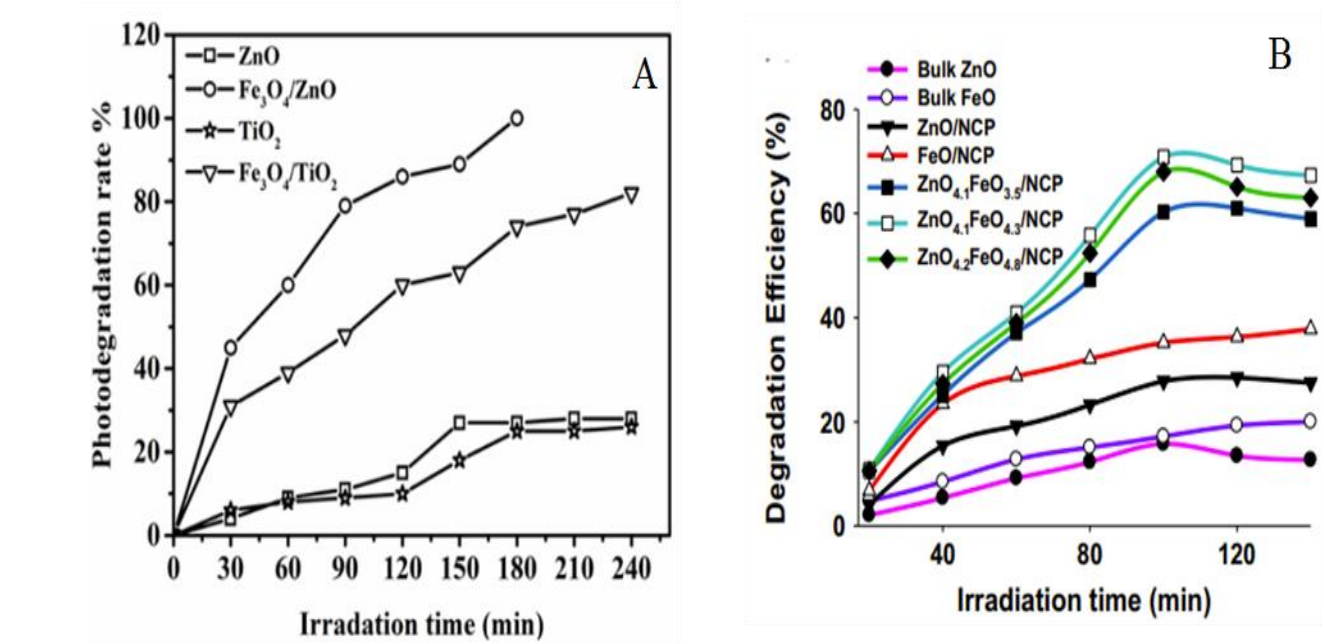


**Fig. 4.** (A) MB dye photodegradation rate [191], (B) wastewater photodegradation rate under visible light [192].

**Table 1.** Modified ZnO semiconducting material for organic dyes degradation.

| Photocatalysts | Dye | Degradation rate % | light | k $(min)^{-1}$ | Time (min) | pH | Ref. |
|---|---|---|---|---|---|---|---|
| ZnO | MB | 35 | UV | - | 90 | 8 | [139] |
| Na-doped ZnO | MB | 99.5 | UV | - | 90 | 8 | [139] |
| Fe doped ZnO | MO | 98.7 | Sunlight | 0.65 | 300 | -- | [140] |
| Cr doped ZnO | MB | 98 | UV | 0.041 | 150 | 7-13 | [141] |
| | MO | ~100 | | 0.0012 | | 3-4 | |
| PAN/ZnO Hybrid Nanofibers | MG | 99 | Visible | 0.0367 | 200 | -- | [127] |
| | MO | 99 | | 0.0274 | 280 | -- | |
| Ag decorated ZnO | Rh-B | 39.26 | Sunlight | -- | 80 | -- | [142] |
| | MB | 80.09 | | -- | 100 | -- | |
| Ag/ZnO core/shell | MB | 100 | Visible | 0.0668 | 90 | 10 | [52] |
| G-ZnO | Rh-B | 100 | Visible | -- | 90 | -- | [143] |
| | MB | 100 | | | 105 | | |
| | MO | 100 | | | 120 | | |
| Mg-ZnO-CNT | MB | 75 | xenon lamp | 0.0875 | 60 | -- | [144] |
| Mg-ZnO-G | | 40 | | 0.0086 | 60 | -- | |
| Ag/ZnO | RhB | 95 | UV | 0.025 | 120 | -- | [145] |
| | | 82 | Visible | 0.0143 | | -- | |
| Au@ZnO | MO | 98 | UV | $10.80\times10^{-2}$ | 40 | -- | [53] |
| | TE | 99 | | -- | 100 | -- | |
| Au/ZnO | Rh-B | 85 | UV | -- | 180 | 6 | [146] |
| Fe/ZnO | MB | -- | Visible | 0.0036 | 75 | -- | [147] |
| Al/ZnO | | -- | | 0.0068 | | -- | |
| Al-Fe/ZnO | | 90 | | 0.014 | | -- | |
| ZnO–CdS core–shell | Congo red | 88 | UV | -- | 75 | 3 | [148] |
| $ZnO/Fe_2O_3$ nanocomposite | GRL | 81.1 | Solar | -- | 200 | 7 | [149] |
| $ZnO/Fe_2O_3$ nanotube composites | MB | 94.25 | UV | -- | 60 | -- | [150] |
| ZnO/ SiNW | MB | 0.4 | UV | -- | 60 | -- | [151] |
| | | 6.7 | Visible | | | | |
| $ZnO:TiO_2$ | MB | 90 | Visible | -- | 75 | -- | [152] |
| ZnO@ZnS | MB | 95 | UV | -- | 120 | 7 | [153] |
| ZnO:Cd | MB | 99 | UV | 0.073 | 60 | -- | [154] |
| St-ZnO | MB | 90 | Sunlight | -- | 45 | -- | [155] |
| Ag-ZnO/g-C3N4/GO | MB | 98.86 | Visible | -- | 15 | -- | [156] |
| Mn-ZnO | MB | 95 | UV | -- | 180 | 10 | [157] |
| α-Fe2O3 – ZnO | MB | 100 | Sun light | 0.036 | ۱۲۰ | -- | [158] |
| W/Ag/ZnO | Turquoise | 55 | Sunlight | -- | 60 | -- | [159] |
| Al/ZnO | Blue | 80 | | | | | |
| CuO/ZnO | MB | 92.4 | UV | -- | 180 | -- | [160] |
| ZnO-Fe | MO | 100 | UV | -- | 180 | -- | [161] |
| $ZnO/Fe_3O_4$ | RhB | 99 | UV | -- | 120 | -- | [162] |

Four different types of the morphology of ZnO nanostructures, namely hexagonal disks, dumbbell-shaped, rice-like, rods, and rice-like morphology which show the highest photodegradation efficiency due to their larger specific surface area and higher defect content of electron trapping than the other nanostructures, up to now observed [74]. Moreover, the photocatalytic activity of a photocatalyst is projected to rise as particle size reduces due to an increase in charge carrier transfer rate and the number of active sites accessible for reaction, as well as an increase in specific surface area. Then, the charge carrier recombination rate can offset activity as a result of increased activity due to a higher specific surface area if the particle size is small

enough [75]. Mauro et al. [76] found that ZnO nanofibers appeared to have 40% higher photodegradation than ZnO thin film and ZnO nanorods due to the large exposed surface area. The ZnO NRs with a growth seed layer of 3 nm showed higher photocatalytic efficiency than ZnO NRs that had a growth seed layer of 30 nm [76]. The porosity interest of other structures of a catalyst material that is effective to improve the photodegradation of dyes or pollutants. Pauporté and Rathouský [77] prepared porous ZnO and found that photodegradation is significantly increased by porous thin films compared to non-porous thin films [77]. Sanchez et al. studied the photodegradation process of various ZnO nanostructures like nanoneedles, nanospheres, and polyhedral-shaped against methyl orange (MO) and safranin O (SAF) dye under UV and noted complete photodegradation of the MO solution for ZnO nanoneedles, polyhedral shaped-ZnO, and ZnO nanosphere powders that were achieved at 20, 40, and 70 min, respectively. However, SAF dye showed slower photodegradation by ZnO nanostructures compared to other dyes [78]. The existence of native defect sites on the surface of ZnO due to oxygen vacancy is thought to play a bigger role in photocatalysis kinetics than crystallite size and surface area [79]. The nanoneedles-ZnO appeared to have the best photocatalytic activity due to the presence of a larger level of native defect sites in these nanostructured powders which might be linked to the occurrence of oxygen vacancies in the ZnO structure because of trapped charge carriers by the vacancies thus, the charge carrier recombination is slowed, which leads to allowing the ZnO nanostructures to contain many more defects near the surface [78]. Furthermore, Hasanpour et al. [80] reported that the surface area is the most important parameter affecting on photocatalytic activity because of more pollutants concentration are being photodegraded as a result of a rise in the high surface area of photocatalysts, it is for the areas where the photocatalytic reaction takes place to increase. **Table 2** lists the effects of ZnO morphology, light, and time on the photodegradation of different organic dyes. Furthermore, A. Sobhani-Nasab et al. [81] found that the degradation ratio increased from 76 to 97% for RB dye when the particle size of $CuMn_2O_4$ nanoparticles was decreased from 25 to 11 nm.

### *3.2 Calcination and annealing temperature*

The calcination temperature has a high effect on increasing the photocatalysis activity of the catalyst

**Table 2.** ZnO nanostructure: method of preparation, size, and various parameters for dye photodegradation.

| ZnO morphology | Dye | Light | k $(min)^{-1}$ | Time(m) | Degradation rate% | Ref. |
|---|---|---|---|---|---|---|
| Hexagonal disks | MB | UV | $8.30x10^{-3}$ | 240 | 91.6 | [74] |
| Dumbbell-shaped | | | $4.40x10^{-3}$ | | 73.4 | |
| Rice-like | | | $1.59x10^{-2}$ | | | |
| Rods | | | $3.30x10^{-3}$ | | 64.7 | |
| Flake | Clitoria ternatea floral | UV | | 40 | 14 | [163] |
| Rod | | | | | 10 | |
| Dot | | | | | 30 | |
| microflower-like 0 | MB | UV | | 180 | 81 | [164] |
| microflower-like1 | | | | | 74 | |
| rod-like 2 | | | | | 100 | |
| rod-like5 | | | | | 100 | |
| microflower-like 0 | MB | Visible light | | 180 | 42 | |
| microflower-like 1 | | | | | 37 | |
| rod-like 2 | | | | | 72 | |
| rod-like 5 | | | | | 98 | |
| NRs/NFs | MB | Sun light | | 270 | 86 | [165] |
| NPs | | | | | 97.4 | |
| hexagonal nanodisks | MB | UV | $8.30 \times 10^{-3}$ | 240 | 91.6 | [74] |
| hexagonal dumbbell-shaped | | | $4.40x10^{-3}$ | | 73.4 | |
| rice-shaped | | | $1.59x\ 10^{-2}$ | | | |
| NRS | | | 3.30x 10-3 | | 64.7 | |
| nanoflakes | MO | UV | $1.5 \times 10^{-2}$ | 90 | - | [166] |
| nanobars | | | $0.65\times10^{-2}$ | | - | |
| scale-like | MB | visible | -- | 120 | 74 to97 | [167] |
| flower-like | | | -- | | 18 to91 | |
| Nanowire | MB | UV | -- | 16 | 99 | [168] |
| Nanoporous | | | -- | 23 | 99 | |

| | | | | | | |
|---|---|---|---|---|---|---|
| NPs | | | -- | 30 | 99 | |
| NRs | | | -- | 35 | 99 | |
| NPs | MB | UV | -- | 79 | 57 | [169] |
| Nanocapsule like | | | -- | 50 | 100 | |
| Honeycomb structure powders | MB | UV | -- | 150 | 22 | [170] |
| Spongy powders | | | -- | | 99 | |

material because increasing temperature leads to improve crystallization of samples, removes unwanted impurities, and reduces water molecules that in turn leads to reducing the active sites on the surface. However, increasing the calcination temperature works to break down the pores that reduce the surface area of the synthesis photocatalyst [82]. It is however, preferable to use a moderate temperature to ensure an increase in the surface area of the photocatalyst, which in turn works to increase the photocatalytic activity, and gives a large surface area for the dye to be absorbed on the surface of the photocatalyst. Enhanced crystallinity of the catalyst allows for less recombination of photo-exited carriers, which leads to increasing photocatalysis activity [73]. Zhang et al. [27] reported that the highest photodegradation rate was achieved at by 350 ˚C for ZnO nanorods are 99.3% at 80 min due to their larger surface area of 8.02 $m^2$/g, while photodegradation of samples at 400, 450, and 500 ˚C was 88.1%, 86.0%, and 56.9%, respectively ˚C. Moreover, ZnO nanorods showed the lowest photocatalytic activity and unstable photodegradation due to the smallest surface area are 7.85, 7.91, and 6.04 $m^2$/g for calcination temperatures of 400, 450, and 500 ˚C, respectively. [27]. He et al. [83] reported that the photocatalytic activity of MO dye of the ZnO sample slightly decreased when the calcination temperature increased from 300 to 400 ˚C but slightly increased when the calcination temperature increased to 500 ˚C. Further increases in temperature up to 600 ˚C had a negligible effect on the activity of the ZnO samples. These results are due to the effect of calcination temperature on the photocatalytic activity of ZnO and may be regarded as to the morphological, surface, and optical properties of the ZnO samples [83]. Hayat et al. [84] referred to the relationship between the particle size and crystallinity with calcination temperature which increases the temperature from 400 ◦C to 500 ◦C and then the photocatalytic activity of phenol dye decreased with a further increase in calcination temperature because of the increase in sintering of crystallites and particle size [84]. Increasing the number of active sites on the photocatalysis surface is the most likely responsible reason for the increase in photocatalytic activity due to the increase in the surface area [85].

Lv et al. [86] reported an increase in the photocatalytic activity of the ZnO thin films with increasing annealing temperature through studies photodegradation of MO dye under three-state annealing at 400, 600, and 800 ˚C. Aryanto et al. [87] have indicated that the reason for the photocatalytic activity is enhanced as the annealing temperature and increases to some extent, which is likely due to the increased grain size of ZnO films. Umar et al. [88] have further studied photodegradation for direct red-23 (DR-23) and it appears the intensity of the absorptions is a steady decrease with UV irradiation time for each annealed ZnO photocatalyst. No significant absorptions for the DR-23 dye under investigation are observed after 110, 90, 80, 90, and 100 min of annealed temperatures at 400, 500, 600, 700, and 800 ˚C, respectively. ZnO photocatalysts observed that photodegradation activity was initially increased with annealing up to 600 ˚C, then a decreasing direction was observed for further increases in annealing temperatures. While Sharma et al. [89] found that the photodegradation efficiency to be higher for ZnO nanoparticles that were annealed at 700 ˚C than as prepared or for those annealed at 300 ˚C due to the simpler charge transfer properties possessed by ZnO that was annealed at 700 ˚C for Eosin Y (EY) dye. Derikvandi and Nezamzadeh-Ejhieh [90] found that the photocatalytic activity of the catalysts first increased when temperature increased from 200 to 600 ˚C of $SnO_2$-ZnO and noted decreasing activity with increasing calcinations temperature to higher than 600 ˚C. The reason for return deference in the particle size and phase composition at change calcinations temperature. Therefore, the preparation or annealing temperature affects the photocatalytic efficiency of metal oxide photocatalysts in the opposite way. It leads to an increase in crystallinity, which in turn leads to an increase in photocatalytic efficiency, but the surface area is reduced, which is a decisive factor that leads to a decrease in the value of efficiency. **Table 3** contains many studies regarding the effect of the annealing temperature of ZnO and various parameters on dye photodegradation.

*3.3 Solution pH*

One of the most important parameters that affect photocatalysis efficiency is the pH, which works to

control the adsorption of organic molecules on the surface of the photocatalyst [91]**.** Photodegradation reactions depend on the ionization state as well as the surface charge of the photocatalyst, which are determined by the pH value in the medium [92]. The features of the material surface charge, molecule charge, organic molecule adsorption on the photocatalyst surface, and the number of hydroxyl radicals all of them have a significant impact on the photocatalytic performance. The photocatalytic activity of various pollutants in wastewater is estimated using pH as a key operational parameter [93]. The adsorption of each dye on the photocatalyst surface changes with pH and the point of zero charges of the photocatalyst various with pH [94]. Some dyes decompose on the surface of the photocatalyst where dye adsorption is a critical stage in the photocatalytic degradation process. Although a dye with a high adsorption rate fades quickly, the number of effect sites for absorbing UV light reduces with adsorption increases [95]. The relationship between pH value and photodegradation efficiency has a better understanding when the point of zero charges (PZC) has been determined by measuring the zeta potential of the most effective sample [96]. Consequently, the surface of the catalyst was negatively charged when pH> pHzpc while positively charged when pH< pHzpc and neutrally case when pH ≈ pHzpc [97]. Furthermore, a higher pH value may result in a higher concentration of hydroxyl ions which react with holes to create hydroxyl radicals leading fast photocatalytic degradation rate for dyes [95]. The photodegradation increase in the basic medium due to an increase in hydroxyl ions which drive the generation of hydroxyl radicals [52]. On the other hand, the effect of pH value on photocatalysis performances can be explained in terms of electrostatic interactions between the photocatalyst surface and the target substrate where such electrostatic interactions can be expected to affect the encounter eventuality of the resultant hydroxyl radicals with the dye. It follows that the overall reaction would be enhanced or hindered depending on whether attractive or repulsive forces prevail [98]. ZnO has a positive surface charge when the pH value is below 9.0 ± 0.3 and a negative charge above it according to Eqs. 25 and 26 [99]:

$$ZnOH + H^+ \rightarrow ZnOH_2^+ \quad 25$$

$$ZnOH + OH^- \rightarrow ZnO^- + H_2O \quad 26$$

Anionic dyes are strongly adsorbed in the acidic medium while cationic dyes are highly adsorbed in the basic medium. However, ZnO dissolves in both extremely acidic media at pH less than 3 and in strongly basic media at pH values higher than 11 because it is an amphoteric oxide according to Eqs. [99]:

$$ZnO + 2H^+ \rightarrow Zn^{2+} + H_2O \quad 27$$

$$ZnO + 2OH^- + H_2O \rightarrow Zn(OH)_4^{2-} \quad 28$$

Habibi and Sardashti [100] found that when the pH is higher than 7, it leads to ZnO being in a formula of $Zn(OH)_4^{2-}$ or $Zn(OH)_3^-$ therefore, the electrostatic interaction with the Methyl orange (MO) radical anion is not preferable at a pH higher than 7. ZnO nanoflowers structure appeared high photocatalytic activity against MB dye of 97% obtained under pH value of 13 through 20 min for [101]. Singh and Dutta reported photodegradation activities of 7.169% and 47.63% for pH values of 4.5 and 10.5 respectively, after 120 min of exposure ZnO nanorods to UV light [102]. Furthermore, Ag/ZnO core/shell catalyst is completely

**Table 3.** Temperature effect of photodegradation organic dye based on ZnO nanostructure.

| Annealing Temperature (˚C) | Dye | Morphology | Degradation rate% | Time (min) | Light | k $(min)^{-1}$ | Ref. |
|---|---|---|---|---|---|---|---|
| 250 | | | 76.72 | | | 0.0180 | |
| 300 | MV | NRs | 78.04 | 90 | Sun light | 0.0181 | [171] |
| 350 | | | 79.67 | | | 0.0184 | |
| 400 | | | 81.30 | | | 0.0189 | |
| 400 | | | 88.48 | | | 0.02580 | |
| 500 | | | 95.49 | | | 0.03348 | |
| 600 | DR-23 | NPs | 100 | 80 | UV | 0.04183 | [88] |
| 700 | | | 92.63 | | | 0.03013 | |
| 800 | | | 86.40 | | | 0.02387 | |
| 400 | | | 84 | | | -- | |
| 800 | MO | NRs | 98 | 120 | UV | -- | [172] |
| 900 | | | 57 | | | -- | |
| 400 | | | 73.4 | | | -- | |
| 600 | MO | NPs | 85.8 | 180 | UV | -- | [86] |
| 800 | | | 88 | | | -- | |

photodegraded MB dye at 90 min for a pH value of 10 under visible light [52]. Whang et al. found that the Ag/ZnO nanoparticles showed photodegradation activity of 35%, 41%, and 92% for pH values of 4, 7, and 11 respectively, with an exposure time of 8 h under visible light [103]. **Table 4** outlines some published works regarding the pH effect on the degradation of ZnO nanostructures by various types of organic dyes.

*3.4 Photocatalyst loading*

Catalyst loading is the most important factor that has on the efficiency and photodegradation rate of photocatalytic activity [104] and this impact is noticed because increasing the catalyst dosage produces a greater number of active sites. Higher electron-hole generation led to enhanced production of hydroxyl and superoxide radicals which aid in the decomposition process. Consequently, increasing the ZnO content, until it reaches an optimal loading, leads to the elimination of emerging pollutants by photocatalytic degradation [105]. However, a higher concentration of the photocatalyst may cause the particles to agglomerate and reduce the homogeneity of the suspension thus, reducing the availability of active sites. It is necessary to use the optimum concentration of the photocatalyst to avoid reducing the efficiency of the photodegradation of pollutants by unfavorable light scattering and reducing light penetration into the solution that may result from solution turbidity [104]. Sanna et al. [106] reported the influence of catalyst loading with different concentrations of ZnO catalyst (0.05-0.75) mg/mL on MO degradation for 2 h and they noted that the MO degradation resulted in 47% in the loading 0.05 mg/mL increased to 82% with increasing the loading ratio of the catalyst to 0.1 mg/mL. Increasing the degradation ratio with loading could be due to increasing the active sites numbers leading to enhance the production of the OH• radical. Li et al. [107] studied using various ZnO loading concentrations into CS/ZnO/GA fiber and noted increasing the degradiation digradiation ratio of MO dye from 3.8%, 4.2%, 5.2%, 6.9% to 7.9% with increasing ZnO ratio in the compound. **Table 5** contains the effect of catalyst loading concentration of different types of ZnO nanostructures on the degradation ratio of various dyes.

*3.5 Light intensity and wavelength*

Light intensity plays a significantly important role in the movement of e- from its valance band to the conduction band, and hence the rate of generation of charge carrier pairs [108]. Thus, light intensity is related to the overall

**Table 4.** Solution pH effect on ZnO semiconducting material for organic dye degradation.

| Dye | pH | k $(min)^{-1}$ | Time (min) | Light | Degradation rate % | Morphology | Ref. |
|---|---|---|---|---|---|---|---|
| MB | 3 | 0.014 | 50 | sunlight | -- | Ag/ZnO NPs | [173] |
| | 6 | 0.025 | 50 | | -- | | |
| | 7 | 0.238 | ~15 | | -- | | |
| | 10 | 0.241 | ~15 | | -- | | |
| Congo red | 4 | -- | 120 | xenon lamp | 85 | ZnO NPs | [174] |
| | 7 | -- | | | 80 | | |
| | 10 | -- | | | 83 | | |
| MB | 8 | 0.0054 | 240 | UV | 71 | ZnO NRs | [20] |
| | 9 | 0.0060 | | | 77 | | |
| | 10 | 0.0075 | | | 87 | | |
| | 11 | 0.0099 | | | 94 | | |
| RB | 4 | -- | | | 96 | | |
| | 8 | / | | | 100 | | |
| | 11 | -- | | | 83 | | |
| MB | 4 | -- | 240 | | 60 | ZnO NPs | [94] |
| | 8 | -- | | | 42 | | |
| | 11 | -- | | | 81 | | |
| BG | 4 | -- | | | 70 | | |
| | 8 | -- | | | 74 | | |
| | 11 | -- | | | 56 | | |
| MB | 13 | -- | 20 | UV | 97 | flower-like ZnO microspheres | [101] |

**Table 5.** Effects of dye type on the photocatalytic degradation of dyes.

| Photocatalysts | Dye | Light source | k $(min)^{-1}$ | Time (min) | Degradation rate% | Ref. |
|---|---|---|---|---|---|---|
| Ir doped ZnO NPs | MB | visible | | 50 | 46 | [175] |
| | crystal violet | | | 60 | 40 | |
| ZnO hexagonal shaped | Benzoic acid | UV | -- | 400 | 65.7 | [176] |
| | MB | | -- | 120 | 98.1 | |
| ZnO mixture (rod and sphere) | 4-NP | Visible | | 330 | 76 | [177] |
| | MB | | | | 95 | |
| | BB | | | | 87 | |
| ZnO hair-like | MB | Sunlight | | | 15 | [178] |
| | MO | | | | 30 | |
| | Rho-B | | | | 35 | |
| | textile effluents | | | | 45 | |
| ZnO NPs | MB | Sunlight | $8.7 \times 10^{-3}$ | 330 | 92 | [179] |
| | ECBT | | $6.7 \times 10^{-3}$ | | 86 | |
| ZnO NRs | MB | 300W solar lamp | 0.00253 | 330 | -- | [102] |
| | Rh 6G | | 0.00269 | | -- | |
| ACS-ZnO (honeycomb porous) | MB | UV | 0.1676 | 120 | 93.3 | [180] |
| | RhB | | 0.05253 | | 88.75 | |
| | NR | | 0.06891 | | 86.6 | |
| ZnO | Red 141 | Solar light | 0.1432 | 20 | | [181] |
| | Congo red | | 0.0494 | 60 | 100 | |

energy input to the photocatalysis process [109]. Therefore, there is an expected increase in the reaction with the increase in light intensity [110]. The photodegradation activity was proportional to the flux of radiant [111] where the photodegradation activity would increase linearly with increasing light intensity when the flux of radian is (0-20) $mW/cm^2$ while the increase will be proportional to the square root of the light intensity when the flux of radian is about 25 $mW/cm^2$. However, when the flux of radian is greater than 25 $mW/cm^2$, the photocatalytic activity is independent of the flux of radian [112]. Ebrahimi et al. indicated that increasing the light intensity from 17.2 to 50.5 $mW/cm^2$ led to an increase in the efficiency of the system from 27.8 to 73.5% after 60 min under UV illumination [113]. Maio et al. [114] studied the effects of light intensity and ZnO nanoparticles dosage on the photocatalytic activity against mordant black 11 dye. They noted that using a relatively low ZnO nanoparticles dosage of 0.15 g/L and light intensity ranging from 7.69 to 11.1 $\mu W/cm^2$ has led to a significant impact on the dye photodegradation. However, when light intensity was higher than 11.1 $\mu W/cm^2$ and 0.3 g/L dosages of ZnO nanoparticles appeared less impact on dye photodegradation. However, Shukla et al. [115] noted that increasing lamp power from 160 W to 330 W led to a decreased time of photodegradation of phenol dye from 4 to 3h using ZnO photocatalysts with an efficiency of 95%. On the other hand, the light wavelength was affected on the photocatalytic efficiency [116]. Hence, UV irradiation, according to its emitting wavelength can be classified into spectrums as UVA (315 to 400 nm), UVB (280 to 315 nm), and UVC (100 to 280 nm) [111]. The average radiation energy is 3.44, 4.13, and 5.28 eV in UVA, UVB, and UVC regions, respectively, and to the best of our knowledge, ZnO photocatalysts adsorb UV irradiation [117]. However, around 5% of sunlight is UV while 43% is a visible light thus, the interest of researchers was focused on developing photocatalysts driven by visible light for successfully employing sunlight irradiation as an unlimited source of energy [118]. Chen et al. [11] found of ZnO particles exhibited a 99.70% degradation rate for MO under UV irradiation which has a 365 nm wavelength while Beura et al. [119] studied the effects of UV and sunlight irradiation on photodegradation efficiencies for methyl orange (MO) with Ag-impregnated ZnO-graphene and found high photocatalytic activity as 98% and 96% were achieved under sunlight and UV. Zouhier et al. [34] reported that

both ZnO and $ZnFe_2O_4$/ZnO presented similar good efficiencies for MB and RB dyes photodegradation under UV irradiation while $ZnFe_2O_4$/ZnO only sample was photoactive under visible irradiation, presenting an excellent performance under these irradiation conditions. Singha et al. [120] found of high highly efficiency of photocatalytic activity of ZnO Micro flower Photocatalyst on MB dye so obtained result degradation of ~96% and 97 under sunlight and UV irradiation, respectively.

## 4. Dye type

With the rapid development of industry, organic dyes have been widely used in many complex industrial applications, so today, they are indispensable. However, dyes and their intermediates can be oxidized, hydrolyzed, or subjected to other chemical reaction processes and result in the generation of potentially hazardous byproducts [121]. Further, the presence of dyes in the waste effluent, even in minute concentration is very undesirable and unpleasant. It has major consequences for aquatic life as well as human health disorders [122]. Thus, the exposure of such polluted water in the human body may also be susceptible to a broad spectrum of immune suppression, and problems for respiratory, central nervous, and neurobehavioural disorders presage as allergy, multiple myeloma, leukemia, tissue necrosis, autoimmune diseases, eye infections, irritation, and even lung edema [102, 103]. Organic dyes are containing two major components: chromophores and auxochromes. The first is responsible for the formation of color which is an electron acceptor and often contains heteroatoms as N, O, and S, with non-bonding electrons. While auxochromes can increase color by improving the color solubility and adhesion of fibers that are electron donors [125]. For this reason, the chemical structure of the organic dyes has a considerable effect on the reactivity of these dyes [126]. Guo et al. studied the photocatalytic degradation of ZnO tetrapods against two dyes are acid orange 7 (AO7) and methyl orange (MO) under UV illumination with the intensity of 66.2 $mW/cm^2$ and they noted that AO7 is more sensitive to radical hydroxyl and was the slowest photodegradation compared by MO that showed less sensitive behavior to radical hydroxyl and fastest photodegradation [79]. On the other hand, the charged surface was highly important in the photocatalytic efficiency case of electrostatic force [127] such as MO is anionic and Malachite green (MG) is cationic dyes and are selected to study the photocatalysis process of ZnO NRs and PAN/ZnO NFs and noted that the negatively ionized anionic dye molecules get repelled from the negatively charged PAN/ZnO hybrid NFs while positively charged dye gets attracted. As a result, the cationic dye was absorbed more on the photocatalyst surface than the anionic dye [127] as seen in **Fig. 5**. Liu et al. reported significant

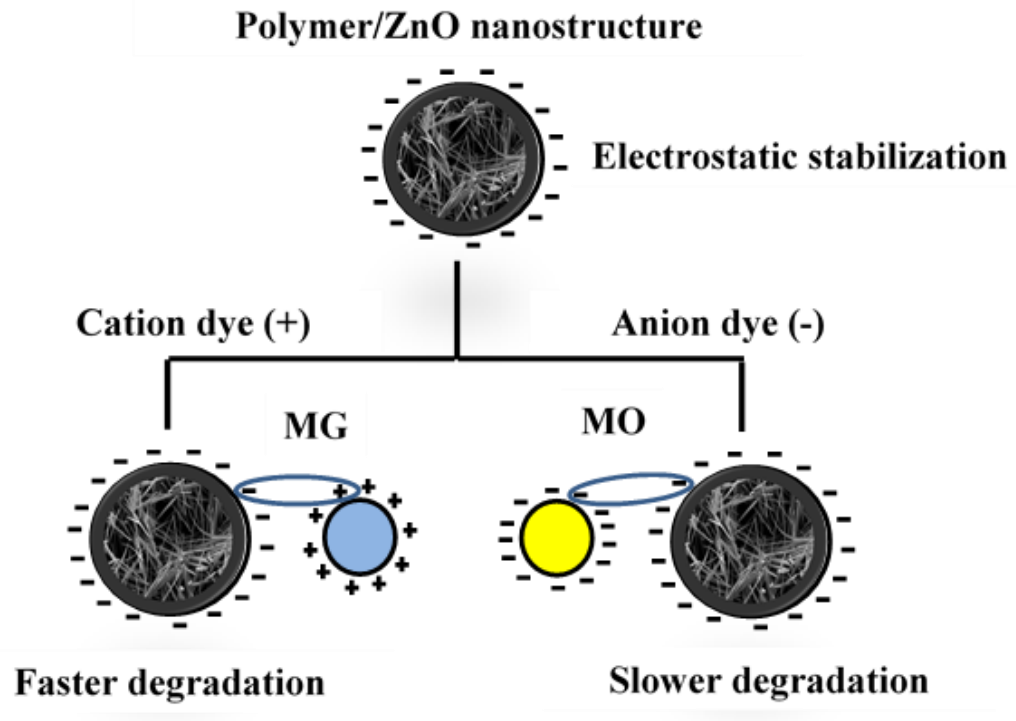


**Fig. 5.** Interaction between dye molecules and PAN/ZnO hybrid NFs [127]

variances in the amount of adsorbed dye and noted the difference in anionic dye adsorption is the attribute to the difference in positively charged site concentration due to the shallow donors. The adsorption of anionic dyes with no positively charged groups was found to be affected by such defect sites [128].

Additionally, the dye's structure is essential because it affects how effectively the photocatalytic mechanism can offend the functional groups and break apart the dye's aromatic ring [129]. The dye's structure was destroyed according to absorbs photons such as MB dye, its dimer, and trimer photons were absorbed at 606 nm and 565 nm respectively, however, the monomer its photon absorbs at 664 and 624 nm. Senobari and a Nezamzadeh-Ejhieh [130] reported that the dimer or trimer can degrade over long periods of time because the intensity of the associated peak at 608 nm tends to weaken over time. Compared to its monomer, the MB dimer exhibits a greater molar absorptivity. This demonstrates that dimers have stronger resonance and stability for eliminating their intermediates [130].

The results of several studies on the effect of dye type on the photoactivity of different dye pollutants are summarized in **Table 6**. The kinetics of the photocatalytic reaction of organic dyes over various photocatalysts follows the Langmuir–Hinshelwood (L–H) model [131]:

$$r = -\frac{dC}{dt} = \frac{kKC}{1+KC} \qquad 29$$

Where r is the reaction rate of the degradation (mg/l min), C is the concentration of the dye (mg/l), t is the illumination time, k is the photodegradation constant (mg/l min), and K is the adsorption coefficient of the reactant on the photocatalyst (l/mg). Since the organic pollutant is millimolar concentration, the product KC is negligible with respect to unity. Eq. 30 can be simplified to an apparent first-order equation [132]:

$$\ln\left(\frac{C_o}{C}\right) = kt \qquad 30$$

Where C◦ is the concentration of initial dye in solution (mg/L), C is the concentration of dye at time t (mg/L), k is the kinetic rate constant (1/min), and t is illumination time (min). In any case, even though it cannot directly provide adequate fitting, the L–H model serves as a foundation for the photocatalytic degradation of organic dyes [133]. The L-H model is based on the monolayer adsorption of both reactants and products in the solid-liquid interface and has been widely utilized to assess the kinetics of typical heterogeneous photocatalytic processes. Additionally, the overall photodegradation process rate-determining stage is the adsorption of these species on the catalyst's surface. The aforementioned adsorption is a process equilibrium in which the degree of oxidant and reductant adsorption has a significant impact on the pollutants and its degradation intermediates photodegradation rates [134]. Many researchers have reported studies on the kinetic rate (k) of organic dyes. Bhatia et al. [135] estimated the k of MO dye of 0.01659 $min^{-1}$ through the use of ZnO NPs as photocatalysts, while Demirci et al. [136] found k value is $1.069x10^{-2}$ $min^{-1}$ of adsorption of MB dyes by ZnO powders prepared by sol-gel route. Zaidi et al. [137] used ZnO nanospheres photocatalysts for

**Table 6.** Photocatalyst loading by ZnO-based photocatalysts

| Photocatalysts | Photocatalyst constriction | Light source | Time (min) | Dye | Degradation rate % | Ref. |
|---|---|---|---|---|---|---|
| ZnO commercial | 0.1 g/l | UV (400 W) | 120 | phenol | 94.6 | [182] |
| ZnO particle commercial | 0.1 g/l | UV (400 W) | 120 | phenol | 85 | [183] |
| ZnO NPs | 5 to 25 gm | mercury vapor lamp (250 W) | 150 | MB | 88 to100 | [184] |
| ZnO (NPs) / Cellulose Nanofibre Composites | $3x10^{-3}$ gm | UV ( 1400-2000 µW/$cm^{-1}$) | 60 | MB | 94 | [185] |
| Carbon-doped ZnO | 300 mg | metal halide lamp (500 W) | 180 | MB | 99 | [186] |
| Cu supported on ZnO (Cylindrical and quasi-spherical shapes) | 150 mg | mercury lamp (400 W) | 30<br>90 | MB<br>MO | 100<br>100 | [187] |
| Cu-doped ZnO (NPs) | 50 mg | Visible light sour (300 W) | 60 | MB | 85 | [188] |

photodegradation of Bismarck Brown R (BBR) dye found the value of kinetic rate (k) was 0.023 $min^{-1}$. Rezaei and Nezamzadeh-Ejhieha [138] reported a value (k) is 0.0915 $min^{-1}$ at 150 min of ZnO/NiO. Its composite synthesis with a definite mole ratio NiO: ZnO, an agate mortar was filled with a suitable quantity of each semiconductor NP. However, different kinetic rate (k) values are obtained when the ZnO nanostructures are used for the degradation of different types of dyes using various pH as listed in **Tables 1-5**.

## 5. Future trends

The preparation of thin films photocatalyst is a very important structure that could be an effective solution to remove oil stains that leak from oil tankers when oil spills in the seas and oceans pose a serious threat to the environment. Oil spills usually float on the surface of the water and this makes their treatment and disposal possible using thin films prepared onto glass substrates. Three important factors may contribute to the success of this model:

1. Preparation of a thin film with a large area to increase the interaction area between the photocatalyst and the organic pollutant.
2. The use of nanostructured thin films will greatly increase the interaction area and nanorods provide this advantage. Further, using thin films will lead to using them more than once which will decrease the cost of water pollution treatment.
3. Make of the photocatalytic process occurs by visible light instead of UV, which makes the photocatalytic process more efficient.

In our lab (unpublished work), we used the low-cost of CBD method to grow ZnO nanorods thin films onto a glass substrate with an area of 15x15cm. **Fig. 6** illustrates the photocatalyst system designed in our Lab., where the reactor is consisting of a stainless steel cylinder with a 34 cm length and 2.2 cm diameter with two outlets for inlet and outlet water. The source of UV irradiation 265 nm provided by the UV lamp is placed inside a cylinder quartz tube and both the UV lamp and the quartz tube are placed inside the stainless steel tube. Then associated with the pump was the FW-070 model**,** 24V DC and the flow rate was fixed at about 1.2 l/min. The pump is working to raise the MB aqueous solution to the reactor from the container through rubber pipes. ZnO nanorods are grown onto the quartz tube for use as a photocatalyst material. The water was contaminated with organic materials (MB dye) contacting ZnO nanorods that grew onto the quartz tube. The obtained results confirmed that the degradation rate increased from 9.63% to 55.4% when the exposure time was increased from 1h to 9h using a pH of 7 to the solution. However, for a pH of 10, the degradation rate is raised to 72.32% after 9h of irradiation. Thus, the designed system showed good results for the degradation of MB dye which made it a promising and cheap way to treat water contaminated with organic matter.

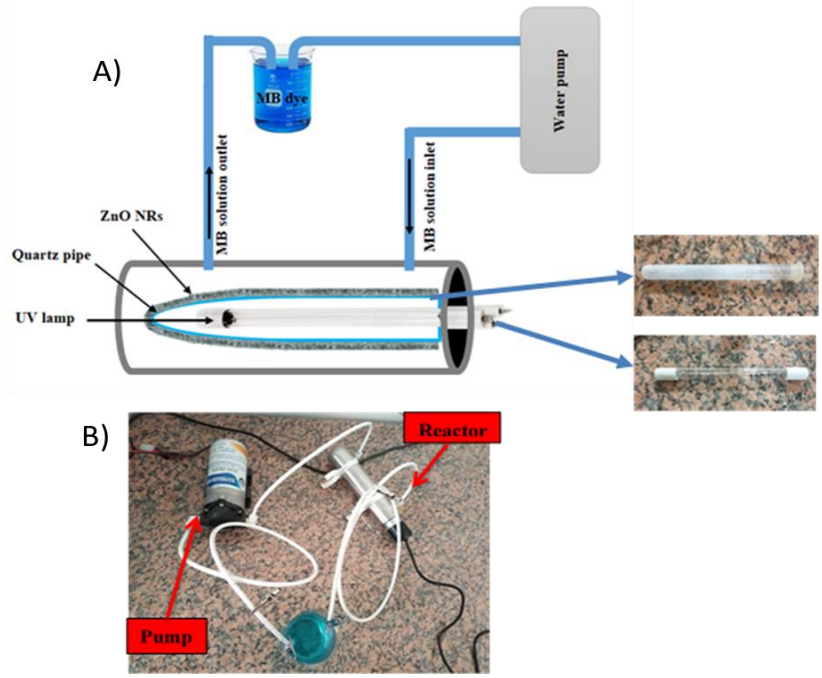


**Fig.6**. (a) Scheme of the designed photocatalytic water flow system (b) photograph of the system [193]

## 4. Conclusions

Metal oxide oxides materials especially ZnO nanostructures are is considered semiconductors materials which used for many applications. However, using ZnO nanostructures to remove organic pollutants from wastewater is one of the important applications due to be a high-quality photocatalyst for the photodegradation of organic dye. ZnO has a wide bandgap of 3.37eV, so it needs UV light to exit electrons to the conduction band and the can be used as a photocatalyst material. Therefore, using ZnO nanostructures as a photocatalyst under visible light is not possible unless modify its surface by coupling or doping with metals such as Ag, Au, and Fe. Found that the ZnO/metal or ZnO/semiconductor nanostructure is increased the photodegradation of various types of dyes under visible light irradiation. There are many important factors that affect the photocatalytic activity of organic dyes. The particles size and shape of the ZnO nanostructures are the most important factor that affect effect on the photodegradation efficiency due to control the high surface-to-volume ratio that almost leads to an increase in the reaction area between the ZnO surface and dye that in turn led to enhance photocatalytic activity. However, nanorods and nanowires ZnO is the interesting structures that appeared high photocatalytic activity compared by others structures. Increasing in the calcination temperature of ZnO nanostructures has been found to enhance the photocatalysis activity of because of improving the crystallinity of the samples. The pH, on the other hand, is one of the most important factors that affect photocatalysis efficiency which works to control the adsorption of the organic molecules on the surface of the photocatalyst and determine the charge of the catalyst. Light intensity plays a significantly important role in the movement of e- from its valance band to the conduction band, and hence the rate of generation of charge carrier pairs. The photodegradation activity would increase linearly with increasing light intensity when the flux of radian is (0-20) $mW/cm^2$ while the increasing will be proportional to the square root of the light intensity when the flux of radian is about 25 $mW/cm^2$. Dye type and structure is the significant parameters that control photocatalytic activity. The chemical structure of the organic dyes has a considerable effect on the reactivity of these dyes.

## Acknowledgements

The authors would like to thank College of Science/University of Basrah for supporting the work.

## References

[1] M. N. Chong, B. Jin, C. W. K. Chow, C. Saint, *Water Res*, 44 (2010) 2997–3027.

[2] A. Ajmal, I. Majeed, R. N. Malik, H. Idriss, M. A. Nadeem, *RSC Adv*, 4 (2014) 37003–37026.

[3] N. N. Mahamuni, Y. G. Adewuyi, *Ultrason Sonochem*, 17 (2010) 990–1003.

[4] R. Andreozzi, V. Caprio, A. Insola, and R. Marotta, *Catal. Today*, 53 (1999) 51–59.

[5] M. S. S. Danish *et al.*, M. S. S. Danish, L. L. Estrella, I. M. A. Alemaida, A. Lisin, N. Moiseev, M. Ahmadi, M. Nazari, M. Wali, H. Zaheb, T, Senjyu, *Metals*, 11 (2021) 1–25,

[6] M. S. S. Danish, A. Bhattacharya, D. Stepanova, A. Mikhaylov, M. L. Grilli, M. Khosravy and Tomonobu Senjyu, *Metals*, 10 (2020) 1–20,

[7] H. Liu, Y. Feng, J. Shao, Y. Chen, Z. L. Wang, H. Li, X. Chen, Z. Bian, *Nano Energy*, 70 (2020), 104499.

[8] S. Vigneshwaran, P. Sirajudheen, C. P. Nabeena, V. P. Sajna, S. Meenakshi, *Int. J. Biol. Macromol*, 183 (2021), 2088–2099.

[9] Y. Zhang, B. Deng, T. Zhang, D. Gao, A. W. Xu, *J. Physic. Chem. C*, 114 (2010) 5073–5079.

[10] M. G. Peleyeju, E. L. Viljoen, *J. Water Process Eng.*, 40 (2021) 101930.

[11] X. Chen, Z. Wu, D. Liu, Z. Gao, *Nanoscale Res Lett*, 12 (2017) 4–13.

[12] Y. Tominaga, T. Kubo, K. Hosoya, *Catal Commun*, 12 (2011) 785–789.

[13] A. Nezamzadeh-Ejhieh, M. Khorsandi, *J Hazard Mater*, 176 (2010) 629–637.

[14] A. Mahmoodi, S. Mahmood Mehdinia, A. Rahmani, H. Nassehinia, *Iran. J. Catal.*, 10 (2020) 23-32.

[15] S. Vahabirad, A. Nezamzadeh-Ejhieh, *J. Solid State Chem*, 310 (2022) 123018.

[16] S. Senobari, A. Nezamzadeh-Ejhieh, *Spectrochim Acta A Mol Biomol Spectrosc*, 196 (2018) 334–343.

[17] M. Willander, *Zinc oxide nanostructures: advances and applications*. Taylor & Francis Group, 2014.

[18] W. A. A. Mohamed, H. T. Handal, I. A. Ibrahem, H. R. Galal, H. A. Mousa, A. A. Labib, *J. Hazard Mater*, 404 (2021) 123962.

[19] D. Upadhaya, D. Dhar Purkayastha, *Ceram Int.*, 46 (2020) 15831–15839.

[20] M. J. Kadhim, M. A. Mahdi, J. J. Hassan, *Mater Inter.*, 2 (2020) 0064–0072.

[21] T. Amakali, Likius. S. Daniel, V. Uahengo, N. Y. Dzade, N. H. de Leeuw, *Crystals*, 10(2020) 132.

[22] Y. I. Choi, H. J. Jung, W. G. Shin, Y. Sohn, *Appl. Surf. Sci.*, 356(2015) 615–625.

[23] J. J. Hassan, M. A. Mahdi, A. Ramizy, H. A. Hassan, Z. Hassan, *Superlattices Microstruct*, 53 (2013) 31–38.

[24] S. Ghattavi, A. Nezamzadeh-Ejhieh, *J. Mol. Liq*., 322 (2021) 114563.

[25] J. J. Hassan, M. A. Mahdi, C. W. Chin, H. Abu-Hassan, Z. Hassan, *Sens. Actuators. B Chem.*, 176 (2013) 360–367.

[26] M. Kamaraj, T. G. Nithya, S. Shyamalagowri, J. Aravind, *Mater Lett.*, 308 (2022) 131128.

[27] X. Zhang, X. Zhang, J. Qin, Y. Xue, P. Yu, B. Zhang, L. Wang, R. Liu, *Sci. Rep.*, 4 (2014) 4596.

[28] J. J. H. Assan, M. A. M. Ahdi, S. J. K. Asim, N. A. M. A. Hamed, *Mater Sci-Pol*, 31 (2013) 180–185.

[29] J. J. Hassan, M. A. Mahdi, C. W. Chin, H. Abu-Hassan, Z. Hassan, *J. Alloys Compd.*, 546 (2013) 107–111.

[30] G. H. Gan Siew Mei, P. Susthitha Menon, *Mater Res. Express*, 7 (2020), 012003.

[31] A. S. Al-Asadi, L. A. Henley, M. Wasala, B. Muchharla, N. Perea-Lopez, V. Carozo, Z. Lin, M. Terrones, K. Mondal, K. Kordas, and S. Talapatra, *J. Appl. Phys.*, 121 (2017), 124303.

[32] R. RatHnasamy, P. Thangasamy, R. Thangamuthu, S. Sampath, V. Alagan, *J. Mater. Sci.: Mater. Elec.*, 28 (2017) 10374–10381.

[33] C. M. Pelicano, H. Yanagi, *Appl. Surf. Sci.*, 506 (2020) 144917.

[34] M. Zouhier, K. Tanji, J. A. Navio, M. C. Hidalgo, A. Kherbeche, *J. Photochem. Photobiol A Chem.*, 390 (2019) 112305.

[35] S. M. Saleh, *Spectrochim Acta A Mol Biomol Spectrosc*, 211 (2019) 141–147.

[36] S. Kumar, R. D. Kaushik, L. P. Purohit, *J. Mol. Liq.*, 327 (2021) 114814.

[37] E. D. M. Isa, K. Shameli, N. W. C. Jusoh, R. Hazan, *J. Nanostructure Chem.*, 11 (2021) 187–202.

[38] V. T. Le, V. D. Doan, T. T. N. Le, M. U. Dao, T-T. T. Vo, H. H. Do, D. Q. Viet, V. A. Tran, *Mater. Lett.*, 283 (2021) 128749.

[39] J. K. Park, J. K. Park, E. J. Rupa, M. H. Arif, J. F. Li, G. Anandapadmanaban, J. P. Kang, M. Kim, J. C. Ahn, R. Akter, D. C. Yang, S. C. Kang, *Optik*, 239 (2021) 166249.

[40] D. Chu, Y. Masuda, T. Ohji, K. Kato, *Langmuir*, 26 (2010) 2811–2815.

[41] M. Y. Guo, A. M. C. Ng, F. Liu, A. B. Djuri, W. K. Chan, H. Su, K. S. Wong, *Journal of Physical Chemistry C*, 115 (2011) 11095–11101.

[42] H. Derikvandi, A. Nezamzadeh-Ejhieh, *J. Hazard Mater*, 321 (2017) 629–638.

[43] M. Mehrali-Afjani, A. Nezamzadeh-Ejhieh, H. Aghaei, *Chem. Phys. Lett.*, 759 (2020) 137873.

[44] A. Yousefi, A. Nezamzadeh-Ejhieh, *Iran. J. Catal.*, 11 (2021) 247-259.

[45] J. T. Mehrabad, M. Partovi, A. Rad, R. Khalilnezhad, *Iran. J. Catal.*, 9 (2019), 233-239.

[46] A. Rostami-Vartooni, A. Moradi-Saadatmand, M. Bagherzadeh, M. Mahdavi, *Iran. J. Catal.*, 9 (2019) 27-35.

[47] H. R. Pouretedal, M. Fallahgar, S. Pourhasan, M. Nasiri, *Iran. J. Catal.*, 7 (2017) 317-326.

[48] J. J. Hassan, M. A. Mahdi, C. W. Chin, H. Abu-Hassan, Z. Hassan, *Physica E Low Dimens Syst. Nanostruct*, 46 (2012) 254–258.

[49] A. Elhalil, R. Elmoubarki, M. Farnane, A. Machrouhi, F.Z. Mahjoubi, M. Sadiq, S. Qourzal, N. Barka, *Environ Nanotechnol Monit Manag*, 10 (2018) 63–72.

[50] W. Bousslama, H. Elhouichet, M. Férid, *Optik*, 134 (2017) 88–98.

[51] S. Majumder, S. Chatterjee, P. Basnet, J. Mukherjee, *Environ Nanotechnol Monit Manag*, 14 (2020) 100386.

[52] M. J. Kadhim, M. Mahdi, J. J. Hassan, A. S. Al-Asadi, *Nanotechnology*, 32 (2021) 195706.

[53] N. L. Gavade, A. N. Kadam, S. B. Babar, A. D. Gophane, K. M. Garadkar, S. W. Lee, *Ceram. Int.*, 46 (2020) 11317–11327.

[54] K. Dib, M. Trari, Y. Bessekhouad, *Appl. Surf. Sci.*, 505 (2020) 144541.

[55] F. M. Sanakousar, C. Vidyasagar, V. M. Jiménez-Pérez, K. Prakash, *Mater Sci Semicond Process*, 140 (2022) 106390.

[56] M. R. Khan, T. W. Chuan, A. Yousuf, M. N. K. Chowdhury, C. K. Cheng, *Catal. Sci. Technol*, 5 (2015) 2522–2531.

[57] C. Ding, K. Fu, Y. Pan, J. Liu, H. Deng, J. Shi, *Catalysts*, 10 (2020) 1–26.

[58] C. M. Magdalane, K. Kanimozhi, M. V. Arularasu, G. Ramalingam, K. Kaviyarasu, *Surfaces and Interfaces*, 17 (2019) 100346.

[59] S. Y. Janbandhu, A. Joshi, S. R. Munishwar, R. S. Gedam, *Appl. Surf. Sci.*, 497 (2019) 143758.

[60] S. Ghattavi, A. Nezamzadeh-Ejhieh, *Compos. B Eng.*, 183 (2020) 107712, 2020.

[61] L. Kong, J. Guo, J. W. Makepeace, T. Xiao, H. F. Greer, W. Zhou, Z. Jiang, P. P. Edwards, *Catal. Today*, 335 (2019) 477–484.

[62] M. A. Mahdi, A. Hmood, A. Kadhim, J. J. Hassan, S. Kasim, Z. Hassan, *Optik*, 127 (2016) 1962–1966.

[63] T. Senasu, T. Chankhanittha, K. Hemavibool, S. Nanan, *Mater. Sci. Semicond. Process*, 123 (2021) 105558.

[64] I. Zgura, N. Preda, G. Socol, C. Ghica, D. Ghica, M. Enculescu, I. Negut, L. Nedelcu, L. Frunza, C.P. Ganea, S. Frunza, *Mater Res. Bull.*, 99 (2018) 174–181.

[65] S. Khanchandani, S. Kundu, A. Patra, A. K. Ganguli, *J. Phys. Chem. C*, 116 (2012) 23653.

[66] J. Aliaga, N. Cifuentes, G. González, C. Sotomayor-Torres, E. Benavente, *Catalysts*, 8 (2018) 1–13.

[67] W. Sun, S. Meng, S. Zhang, X. Zheng, X. Ye, X. Fu, S. Chen, *Journal of Physical Chemistry C*, 122 (2018) 15409–15420.

[68] C. Dong, X. Xiao, G. Chen, H. Guan, Y. Wang, *Mater Chem. Phys.*, 155 (2015) 1–8.

[69] S. Chen, W. Zhao, W. Liu, S. Zhang, *Appl. Surf. Sci.*, 255 (2008) 2478–2484.

[70] S. Ghattavia, A. Nezamzadeh-Ejhiehm, Desalination and Water Treatment, 166 (2019) 92-104.

[71] S. Ahmed, *Crit. Rev. Environ. Sci. Technol*, 42 (2012) 601–675.

[72] F. Zuo, K. Bozhilov, R. J. Dillon, L. Wang, P. Smith, X. Zhao, C. Bardeen, P. Feng, *Angewandte Chemie International Edition*, 51 (2012) 6223–6226.

[73] J. Zhang, B. Tian, L. Wang, M. Xing, J. Lei, *Photocatalysis: fundamentals, materials and applications*, Springer, 2018.

[74] N. M. Flores, U. Pal, R. Galeazzi, A. Sandoval, *RSC Adv.*, 4 (2014) 41099–41110.

[75] A. C. Dodd, A. J. McKinley, M. Saunders, T. Tsuzuki, *J. Nanopart. Res.*, 8 (2006) 43–51.

[76] A. Di Mauro, M. E. Fragalà, V. Privitera, G. Impellizzeri, *Mater. Sci. Semicond. Process*, 69 (2017) 44–51.

[77] T. Pauporté and J. Rathouský, *Journal of Physical Chemistry C*, 111 (2007) 7639–7644.

[78] F. A. L. Sánchez, A. S. Takimi, F. S. Rodembusch, C. P. Bergmann, *J Alloys Compd*, 572 (2013) 68–73.

[79] M. Y. Guo, A. M. Ching Ng, F. Liu, A. B. Djuri, W. K. Chan, H. Su, K. S. Wong, *J. Physic. Chem. C*, 115 (2011) 11095–11101.

[80] M. Hasanpour, S. Motahari, D. Jing, M. Hatami, *Topics in Catalysis*, 2021, https://doi.org/10.1007/s11244-021-01476-3

[81] A. Sobhani-Nasab, M. Eghbali-Arani, S. Mostafa Hosseinpour-Mashkani, F. Ahmadi, M. Rahimi-Nasrabadi, V. Ameri, *Iran. J. Catal*.,10 (2020), 91-99.

[82] T. An, J. Liu, G. Li, S. Zhang, H. Zhao, X. Zeng, G. Sheng, J. Fu, *Appl. Catal. A Gen.*, 350 (2008) 237–243.

[83] L. He, Z. Tong, Z. Wang, M. Chen, N. Huang, W. Zhang, *J. Colloid Interface Sci.*, 509 (2018) 448–456.

[84] K. Hayat, M. A. Gondal, M. M. Khaled, S. Ahmed, A. M. Shemsi, *Appl. Catal. A Gen.*, 393 (2011) 122–129.

[85] N. Horzum, M. E. Hilal, T. Isik, *New Journal of Chemistry*, 42 (2018) 11831–11838.

[86] J. Lv, W. Gong, K. Huang, J. Zhu, F. Meng, X. Song, Z. Sun, *Superlattices Microstruct*, 50 (2011) 98–106.

[87] D. Aryanto, E. Hastuti, M. Taspika, K. Anam, I. Isnaeni, W. B. Widayatno, A. S. Wismogroho, P. Marwoto, B. W. Nuryadin, A. Noviyanto, S. Sugianto, *J. Solgel. Sci. Technol.*, 96 (2020) 226–235.

[88] A. Umar, R. Kumar, G. Kumar, H. Algarni, S. H. Kim, *J. Alloys. Compd.*, 648 (2015) 46–52.

[89] N. Sharma, R. Jha, S. Baghel, D. Sharma, *J. Alloys. Compd.*, 695 (2017) 270–279.

[90] H. Derikvandi, A. Nezamzadeh-Ejhieh, *J. Mol. Catal. A Chem.*, 426 (2017) 158–169.

[91] H. chao Liang, X. zhong Li, Y. hua Yang, K. hung Sze, *Chemosphere*, 73 (2008) 805–812.

[92] S. Ahmed, M. G. Rasul, W. N. Martens, R. Brown, M. A. Hashib, *Water Air Soil Pollut*, 215 (2011) 3–29.

[93] A. A. El-Bindary, S. M. El-Marsafy, A. A. El-Maddah, *J Mol Struct*, 1191 (2019) 76–84.

[94] I. Kazeminezhad, A. Sadollahkhani, *J. Mater. Sci.: Mater. Electronics*, 27 (2016) 4206–4215.

[95] X. Li, Y. Hou, Q. Zhao, L. Wang, *J Colloid Interface Sci*, 358 (2011) 102–108.

[96] M. I. A. A. Maksoud, G. S. El-Sayyad, A. M. El-Khawaga, M. Abd Elkodous, A. Abokhadra, M. A. Elsayed, M. Gobara, L.I. Soliman, H.H. El-Bahnasawy, A.H. Ashour, *J. Hazard Mater*, 3894 (2020) 123000.

[97] A. Eslami, A. Oghazyan, M. Sarafraz, *Iran. J. Catal*. ,8 (2018) 95-102.

[98] R. Comparelli, E. Fanizza, M. L. Curri, P. D. Cozzoli, *Appl. Catal. B*, 60 (2005) 1–11.

[99] G. K. Weldegebrieal, *Inorg. Chem. Commun.*, 120 (2020) 108140.

[100] M. H. Habibi, M. K. Sardashti, *J. Adv. Oxid. Tech.*, 12 (2009) 231–237.

[101] Y. Wang, Y. Yang, L. Xi, X. Zhang, M Jia, H. Xu, H. Wu, *Mater. Lett.*, 180 (2016) 55–58.

[102] R. Singh, S. Dutta, *Nano-Structures and Nano-Objects*, 18 (2019) 100250.

[103] T. J. Whang, M. T. Hsieh, H. H. Chen, *Appl. Surf Sci*, 258 (2012) 2796–2801.

[104] A. Mirzaei, Z. Chen, F. Haghighat, L. Yerushalmi, *Sustain Cities Soc*, 27 (2016) 407–418.

[105] A. B. Patil, K. R. Patil, S. K. Pardeshi, *J. Hazard Mater.*, 183 (2010) 315–323.

[106] V. Sanna, N. Pala, V. Alzari, D. Nuvoli, M. Carcelli, *Mater. Lett.*, 162 (2016) 257–260.

[107] H. Li, M. X. Hao, H. R. Kang, L. Q. Chu, *Int. J. Biol. Macromol*, 181 (2021) 150–159.

[108] L. V Bora and R. K. Mewada, *Renewable and Sustainable Energy Reviews*, 76 (2017) 1393–1421.

[109] S. M. Lam, J. C. Sin, A. Z. Abdullah, A. R. Mohamed, *Desalination Water Treat.*, 41 (2012) 131–169.

[110] J. Guo, C. Dong, J. Zhang, Y. Lan, *Sep. Purif. Technol.*, 143 (2015) 27–31.

[111] K. M. Lee, C. W. Lai, K. S. Ngai, J. C. Juan, *Water Res.*, 88 (2016) 428–448.

[112] H. Zeghioud, N. Khellaf, H. Djelal, A. Amrane, *Chem. Eng. Commun.*, 6445 (2016) 1563–5201.

[113] R. Ebrahimi, A. Maleki, Y. Zandsalimi, R. Ghanbari, *J. Indust. Eng. Chem.*, 73 (2019) 297–305.

[114] J. Miao, Z. Jia, H. B. Lu, D. Habibi, L. C. Zhang, *J. Taiwan Inst. Chem. Eng.*, 45 (2014) 1636–1641.

[115] P. R. Shukla, S. Wang, H. M. Ang, M. O. Tadé, *Sep. Purif. Technol.*, 70 (2010) 338–344.

[116] A. Lais, M. A. Gondal, M. A. Dastageer, F. F. Al-Adel, *Int. J. Energy Res.*, 42 (2018) 2031–2049.

[117] A. Gholamhosseini, K. Nasouri, A. M. Shoushtari, F. Mirgoli, *Fibers and Polymers*, 21 (2020) 1704–1712.

[118] A. A. Yaqoob, N. H. B. M. Noor, A. Serrà, M. N. M. Ibrahim, *Nanomaterials*, 10 (2020) 1–26.

[119] R. Beura, R. Pachaiappan, T. Paramasivam, *J. Physic. Chem. Solids*, 148 (2020) 109689.

[120] M. K. Singha, A. Patra, *Opt. Mater.*, 107 (2020) 110000.

[121] A. R. Khataee, M. Zarei, L. Moradkhannejhad, *Desalination*, 258 (2010) 112–119.

[122] A. R. Khataee, M. B. Kasiri, *J. Mol. Catal. A Chem.*, 328 (2010) 8–26.

[123] K. Y. Foo, B. H. Hameed, *Adv. Colloid Interface Sci.*, 159 (2010) 130–143.

[124] B. H. Hameed, A. T. M. Din, A. L. Ahmad, *J. Hazard Mater.*, 141 (2007) 819–825.

[125] M. Hasanpour, M. Hatami, *J. Mol. Liq.*, 309 (2020) 113094.

[126] A. Khatri, M. H. Peerzada, M. Mohsin, M. White, *J. Clean. Prod.*, 87 (2015) 50–57.

[127] A. P. Shah, S. Jain, V. J. Mokale, N. G. Shimpi, *J. Indust. Eng. Chem.*, 77 (2019) 154–163.

[128] F. Liu, Y. H. Leung, A. B. Djurišić, A. M. C. Ng, W. K. Chan, *Journal of Physical Chemistry C*,117 (2013) 12218–12228.

[129] R. Vinu, S. U. Akki, G. Madras, *J. Hazard Mater*, 176 (2010) 765–773.

[130] S. Senobari, A. Nezamzadeh-Ejhieh, *J. Mol. Liq.*, 257 (2018) 173–183.

[131] Z. D. Li, H. L. Wang, X. N. Wei, X. Y. Liu, Y. F. Yang, W. F. Jiang, *J. Alloy. Comp.*, 659 (2016) 240-247.

[132] S. Chowdhury, Y. Jiang, S. Muthukaruppan, R. Balasubramanian, *Carbon N Y*, 128 (2018) 237–248.

[133] F. F. Brites, V. S. Santana, N. R. C. Fernandes-Machado, *Top. Catal.*, 54 (2011) 264–269.

[134] A. Noruozi, A. Nezamzadeh-Ejhieh, *Chem. Phys. Lett.*, 752 (2020) 137587.

[135] S. Bhatia, N. Verma, *Mater. Res. Bull.*, 95 (2017) 468–476.

[136] S. Demirci, T. Dikici, M. M. Tünçay, N. Kaya, *Appl. Surf. Sci.*, 507 (2020) 145083.

[137] Z. Zaidi, S. I. Siddiqui, B. Fatima, S. A. Chaudhry, *Mater. Res. Bull.*, 120 (2019) 110584.

[138] M. Rezaei, A. Nezamzadeh-Ejhieha, *Int. J. Hydrogen Energy*, 45 (2020) 24749–24764.

[139] M. H. Elsayed, T. M. Elmorsi, A. M. Abuelela, A. E. Hassan, A. Z. Alhakemy, M. F. Bakr, H-H. Chou, *J. Taiwan Inst. Chem. Eng.*, 115 (2020) 187–197.

[140] I. N. Reddy, C. V. Reddy, M. Sreedhar, J. Shim, M. Cho, D. Kim, *Mater. Sci. Eng. B Solid State Mater. Adv. Technol.*, 240 (2019) 33–40.

[141] J. Chen, Y. Xiong, M. Duan, X. Li, J. Li., S. Fang, S. Qin, R. Zhang, *Langmuir*, 36 (2020) 520–533.

[142] M. S. Khan, P. P. Dhavan, B. L. Jadhav, N. G. Shimpi, *Chemistry Select*, 5 (2020) 12660–12671.

[143] M. Maruthupandy, P. Qin, T. Muneeswaran, G. Rajivgandhi, F. Quero, J. M. Song, *Mater. Sci. Eng. B Solid State Mater. Adv. Technol.*, 254 (2020) 114516.

[144] I. Ahmad, M. S. Akhtar, E. Ahmed, M. Ahmad, *Sep. Purif. Technol.*,245 (2020) 116892.

[145] T. N. Q. Trang, T. B. Phan, N. D. Nam, V. T. H. Thu, *ACS Appl. Mater Interfaces*, 12 (2020) 12195–12206.

[146] M. Ahmad, W. Rehman, M. M. Khan, M. T. Qureshi, A. Gul, S. Haq, R. Ullah, A. Rab, F Menaa, *J. Environ. Chem. Eng.*, 9 (2021) 104725.

[147] N. R. Khalid, A. Hammad, M.B. Tahir, M. Rafique, T. Iqbal, G. Nabi, M.K. Hussain, *Ceram. Int.*, 45 (2019) 21430–21435.

[148] M. H. Habibi, M. H. Rahmati, *Spectrochim Acta A Mol Biomol Spectrosc*, 137 (2015) 160–164.

[149] F. S. Hashim, A. F. Alkaim, S. M. Mahdi, A. H. Omran Alkhayatt, *Composites Communications*, 16 (2019) 111–116.

[150] Y. Liu, L. Sun, J. Wu, T. Fang, R. Cai, A. Wei, *Mater Sci Eng B Solid State Mater Adv Technol*, 194 (2015) 9–13.

[151] J. Lan, B. He, C. Haw, M. Gao, I. Khan, R. Zheng, S. Guo, J. Zhao, Z. Wang, S. Huang, S. Li, J. Kang, *Appl. Surf. Sci.*, 529 (2020) 147023.

[152] G. K. Upadhyay, J. K. Rajput, T. K. Pathak, V. Kumar, L. P. Purohit, *Vacuum*, 160 (2019) 154–163.

[153] M. F. Sanad, A. E. Shalan, S. M. Bazid, S. M. Abdelbasir, *J. Environ. Chem. Eng.*, 6 (2018) 3981–3990.

[154] M. Franco, O. Marin, N. C. Vega, L. Tereschuk, D. Comedi, *Materials Latters*, 311 (2022) 131634.

[155] D. Bharathi, D. Bharathi, J. G. T. Nandagopal, R. Rajamani, S. Pandit, D. Kumar, B. Pan t, S. Pandey, P. K. Gupta, *Mater. Lett.*, 311 (2022) 131637.

[156] Z. Habibollahi, M. Peyravi, S. Khalili, M. Jahanshahi, *Mater Today Chem.*, 23 (2022) 100748.

[157] D. A, R. Yadav, S. P. C, *Mater Today Proc.*, 48 (2022) 494–501.

[158] D. K. L. Harijan, S. Gupta, S. K. Ben, A. Srivastava, J. Singh, V. Chandra, *Physica B Condens Matter*, 627 (2021) 413567.

[159] S. Noreen, S. Zafar, I. Bibi, M. Amami, M.A.S. Raza, F. H. Alshammari, Z.M. Elqahtani, B.I. Basha, N. Alwad a, A. Nazir, M.I. Khan, M. Iqbal, *Ceram Int*, 48 (2022) 12170-12183.

[160] X. Wang, M. Deng, Z. Zhao, Q. Zhang, Y. Wang, *Mater Chem. Phys.*, 276 (2022) 125305.

[161] M. Le, H. Suo, G. Tang, H. Qiao, Z. Zhao, N. Martin, *Mater Chem. Phys.*, 275 (2022) 125304.

[162] D. Zhang, X. Zuo, W. Gao, H. Huang, H. Zhang, T. Cong , S. Yang, J. Zhang, L. Pan, *Mater Res. Bull.*, 148 (2022) 111677.

[163] I. J. Peter, E. Praveen, G. Vignesh, P. Nithiananthi, *Mater Res. Express*, 4 (2017) 0–18.

[164] S. Suwanboon, P. Amornpitoksuk, C. Randorn, *Ceram Int.*, 45 (2019) 2111–2116.

[165] K. N. Abbas, N. Bidin, *Appl. Surf. Sci.*, 394 (2017) 498–508.

[166] N. S. Portillo-Vélez, A. Hernández-Gordillo, M. Bizarro, *Catal. Today*, 287 (2017) 106–112.

[167] Y. Lin, H. Hu, Y. H. Hu, *Appl. Surf. Sci.*, 502 (2020) 144202.

[168] M. Vossoughi, F. Ghanbari, A. Simchi, R. Shidpour, *Appl. Catal. A Gen*, 472 (2014) 198–204.

[169] M. Pudukudy, A. Hetieqa, Z. Yaakob, *Appl. Surf. Sci.*, 319 (2014) 221–229.

[170] H. Vahdat Vasei, S. M. Masoudpanah, M. Adeli, M. R. Aboutalebi, M. Habibollahzadeh, *Mater Res. Bull.*, 117 (2019) 72–77.

[171] J. Prince Richard, I. Kartharinal Punithavathy, S. Johnson Jeyakumar, M. Jothibas, P. Praveen, *J. Mater. Sci.: Mater. Electronics*, 28 (2017) 4025–4034.

[172] C. Tian, Q. Zhang, A. Wu, M. Jiang, B. Jiang, H. Fu, *Chem. Commun.*, 48 (2012) 2858–2860.

[173] Y. Liu, Q. Zhang, M. Xu, H. Yuan, Y. Chen, J. Zhang, K. Luo, J. Zhang, B. You, *Appl. Surf. Sci.*, 476 (2019) 632–640.

[174] R. E. Adam, G. Pozina, M. Willander, O. Nur, *Photonics Nanostruct*, 32 (2018) 11–18.

[175] M. Dhanalakshmi, K. Saravanakumar, S. L. Prabavathi, V. Muthuraj, *Inorg. Chem. Commun.*, 111 (2020) 107601.

[176] R. D. Suryavanshi, S. V. Mohite, A. A. Bagade, S. K. Shaikh, J. B. Thorat, K. Y. Rajpure, Mate. Res. Bull., 101 (2018) 324-333.

[177] S. A. Ansari, M. M. Khan, S. Kalathil, A. Nisar, J. Lee, M. H. Cho, *Nanoscale*, 5 (2013) 9238–9246.

[178] P. Dhandapani, A. A. Prakash, M. S. AlSalhi, S. Maruthamuthu, S. Devanesan, A. Rajasekar, *Mater. Chem. And Phys.*, 243 (2020) 122619.

[179] M. Golmohammadi, M. Honarmand, S. Ghanbari, *Spectrochim Acta A Mol Biomol Spectrosc*, 229 (2020) 117961.

[180] C. Qian, J. Yin, J. Zhao, X. Li, S. Wang, Z. Bai, T. Jiao, *Colloids Surf. A Physicochem Eng. Asp.*, 610 (2021) 125752.

[181] T. Sansenya, N. Masri, T. Chankhanittha, T. Senasu, J. Piriyanon, S. Mukdasai, S. Nanan, *J. Physic. Chem. Solids*, 160 (2022) 110353.

[182] K. P. Jyothi, S. Yesodharan, E. P. Yesodharan, *Ultrason Sonochem*,21 (2014) 1787-1796.

[183] S. G. Anju, S. Yesodharan, E. P. Yesodharan, *Chem. Eng. J.*, 189–190 (2012) 84–93.

[184] F. A. Alharthi, A. A. Alghamdi, A. A. Alothman, Z. M. Almarhoon, M. F. Alsulaiman, N. Al-Zaqri, *Crystals* , 10 (2020) 441.

[185] M. Dehghani, H. Nadeem, V. S. Raghuwanshi, H. Mahdavi, M. M. B. Holl, W. J. Batchelor, *ACS Appl. Nano Mater.*, 3 (2020) 10284–10295.

[186] X. Zhang, J. Qin, R. Hao, L. Wang, X. Shen, R. Yu, S. Limpanart, M. Ma, R. Liu, *J. Physic. Chem. C*, 119 (2015) 20544−20554.

[187] A. G. Acedo-Mendoza, A. Infantes-Molina, D. Vargas-Hernandez, C. A. Chavez-Sanchez, E. Rodríguez-Castellon, J. C. Tanori-Cordova, *Mater. Sci. Sem. Process*, 119 (2020) 105257.

[188] S. Sriram, K. C. Lalithambika, A. Thayumanavan, *Optik*, 139 (2017) 299–308.

[189] M. Samadi, M. Zirak, A. Naseri, E. Khorashadizade, A. Z. Moshfegh, *Thin Solid Films*, 605 (2016) 2–19.

[190] X. Zhang, Y. Wang, F. Hou, H. Li, Y. Yang, X. Zhang, Y. Yang, Y. Wang, *Appl. Surf. Sci.*, 391 (2017) 476–483.

[191] M. J. Kadhim, F. Allawi, M. A. Mahdi, S. N. Abaas, *Iran. J. Mater. Sci. Eng.*, 19 (2022) 1–15.

[192] M. Bahrami, A. Nezamzadeh-Ejhieh, *Mater. Sci. Sem. Process*, 27 (2014) 833–840.

[193] M. J. Kadhim, Synthesis and Characterization of Metal oxide Nanostructures Photocatalyst for Environmental and Energy Applications, thesis of PhD, University of Basrah, College of Science, Physics of Department,2020.